PCCP

PAPER

View Article Online
View Journal | View Issue

Cite this: *Phys. Chem. Chem. Phys.*, 2018, **20**, 2761

Electro-click construction of hybrid nanocapsule films with triggered delivery properties†

Flavien Sciortino, ‡*[a] Gaulthier Rydzek, ‡*[b] Fabien Grasset,[c] Myrtil L. Kahn,[d] Jonathan P. Hill,[b] Soizic Chevance,[a] Fabienne Gauffre[a] and Katsuhiko Ariga[be]

Hollow nanocapsules (named Hybridosomes®) possessing a polymer/nanoparticle shell were used to covalently construct hybrid films in a one-pot fashion. The alkyne bearing organic/inorganic Hybridosomes® were reticulated with azide bearing homobifunctional polyethyleneglycol (PEG) linkers, by using an electro-click reaction on F-SnO_2 (FTO) electrodes. The coatings were obtained by promoting the Cu(I)-catalyzed click reaction between alkyne and azide moieties in the vicinity of the electrode by the electrochemical generation of Cu(I) ions. The physicochemical properties of the covalently reticulated hybrid films obtained were studied by SEM, AFM, UV-vis and fluorescence spectroscopy. The one-pot covalent click reaction between the nanocapsules and the PEG linkers in the film did not affect the desirable features of the Hybridosomes® *i.e.* their hollow nanostructure their chemical versatility and their pH-sensitivity. Consequently, both the composition and the cargo-loading of the Hybridosomes® films could be tuned, demonstrating the versatility of these hybrid coatings. For example, the Hybridosome® films were used to encapsulate and release a bodipy fluorescent probe in response to either a pH drop or the application of an oxidative +1 V potential (*vs.* Ag/AgCl) at the substrate. By advancing the field of electro-synthesized films a step further toward the design of complex physicochemical interfaces, these results open perspectives for multifunctional coatings where chemical versatility, controllable stability and a hollow nanostructure are required.

Received 7th November 2017,
Accepted 15th December 2017

DOI: 10.1039/c7cp07506e

rsc.li/pccp

1. Introduction

Over the past several decades, the continuous development of smart and active interfaces has highlighted the requirement for multifunctional coatings. This has triggered the development of several deposition strategies including layer-by-layer films,[1] self-assembled monolayers,[2,3] and various electro-synthesis techniques[4–6] with applications in fields including biomaterials[7] and energy storage.[8] In this regard, two main challenges have emerged: achieving the one-pot deposition of coatings and controlling their structure at the nanoscale.[9–12] For instance, films containing nanocapsules have attracted significant interest as they allow developing biomaterials,[13] sensors,[14] and energy storage devices. For the latter application, the use of porous capsules deposited over electrodes enables accommodating the large volume change accompanying the electrochemical cycles.[15] In the case of delivery devices, the surface trapping of intact vesicles or nanocapsules remains a challenge for preserving their cargo.[16] Indeed, membrane rupture may occur, and in this regard the mechanical properties of the capsule are important. For applications that rely on the amount of released substances, such as drug delivery or sensors, improving the loading capacity of the film is beneficial. To this aim, 3D constructs obtained by direct immobilization of capsules are desirable.[17] Early attempts included the layer-by-layer deposition of cerasome and liposome-containing films.[18–20] Here we report on the one-pot construction of hybrid hollow nanocapsule films that are able to release their encapsulated cargo in response to either a pH or an electrochemical stimulus. The recently reported 100 nm diameter hybrid nanocapsules, named Hybridosomes®,[21,22] have been used as hollow building blocks for assembling the film by reticulation *via* a localized coupling reaction. Possessing an

[a] *University of Rennes, Centre National de la Recherche Scientifique (CNRS, France), Institut des Sciences Chimiques de Rennes (ISCR), UMR 6226, F-35000 Rennes, France. E-mail: flavien.sciortino@univ-rennes1.fr*
[b] *World Premier International (WPI) Research Center for Materials Nanoarchitectonics (MANA), National Institute for Materials Science (NIMS), 1-1 Namiki, Tsukuba 305-0044, Japan. E-mail: RYDZEK.Gaulthier@nims.go.jp*
[c] *CNRS UMI 3629 CNRS – Saint Gobain – NIMS, Laboratory for Innovative Key Materials and Structures (LINK), National Institute for Materials Science (NIMS), 1-1 Namiki, Tsukuba 305-0044, Japan*
[d] *Laboratoire de Chimie de Coordination UPR8241 CNRS, 205 rte de Narbonne, 31000 Toulouse Cedex 04, France*
[e] *Graduate School of Frontier Sciences, The University of Tokyo, Kashiwa 277-0827, Japan*

† Electronic supplementary information (ESI) available: TEM tomography, NTA scattering, NMR, ATR-FT IR spectroscopy, UV-visible spectroscopy, S(T)EM, EDX, CV, AFM and fluorescence spectroscopy analysis. See DOI: 10.1039/c7cp07506e

‡ These authors contributed equally.

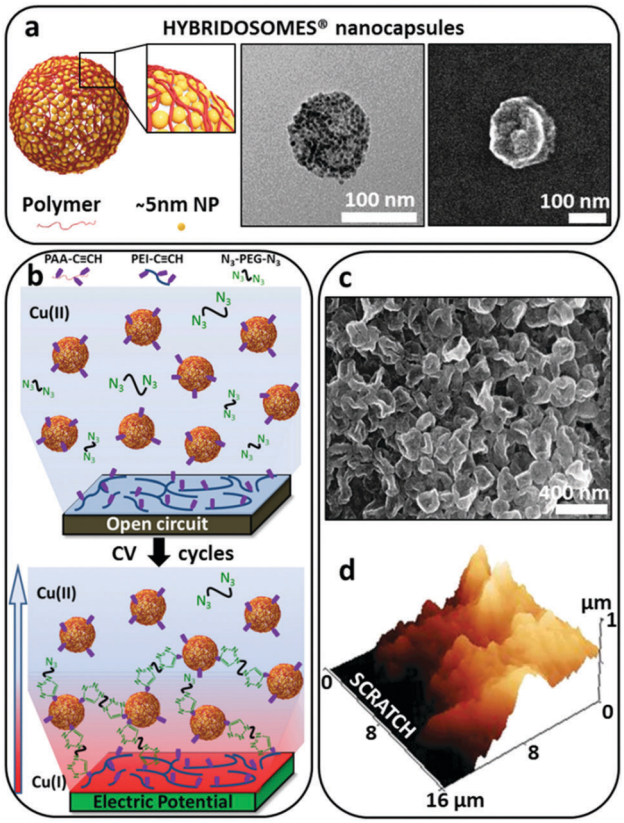

Fig. 1 Concept of Hybridosomes® films covalently assembled by using electro-click chemistry. (a) Schematic depiction, TEM and SEM of deflated hybridosome nanocapsules composed of iron oxide nanoparticles (IONPs) and polyacrylic acid. (b) Schematic representation of the electro-click process, allowing the construction of films on PEI–C≡CH pre-coated electrodes, by using alkyne-functionalized hybridosomes and azide homobifunctional PEG linkers as building blocks in the presence of an electrogenerated Cu(I) catalyst. (c) SEM micrograph of a typical hybridosome film in the dried state. The film was constructed by electro-click after 800 CV cycles (−0.2 V to 0.6 V *vs.* Ag/AgCl, 50 mV s^{-1}) in the presence of 4.5 × 10^9 hybridosomes per mL, 0.1 mg mL^{-1} N_3-PEG-N_3 and 0.6 mM $CuSO_4$ at pH 3.5. (d) Typical 3D view of the corresponding scratched film measured by AFM in the dry state and contact mode.

hybrid shell composed of 5 nm inorganic nanoparticles (NPs) crosslinked by polyacrylic acid (Fig. 1a and Fig. S1, Video S1, ESI†), hybridosomes represent a new class of hollow nanocarriers with several levels of versatility arising from the individual characteristics of their organic and inorganic components and from their hollow structure. For instance, these versatile nanocapsules can be prepared from iron oxide nanoparticles (IONPs), gold nanoparticles, quantum dots (QDs) and their mixtures. The polymer crosslinkers in hybridosomes can be chemically modified to append a chemical recognition or reactive function. These capsules exhibit a narrow size distribution (*ca.* 100 nm in diameter) and their core can be used to encapsulate substances. In addition, they exhibit outstanding mechanical properties, combining deformability and memory shape recovery.[23] To assemble the film in one pot, hybridosomes bearing alkyne moieties (functional polyacrylic acid PAA–C≡CH) were reticulated by electro-click reaction with azide bearing homobifunctional polyethyleneglycol (N_3-PEG-N_3) linkers on F-SnO_2 (FTO) electrodes. A poly(ethyleneimine)-alkyne (PEI–C≡CH) pre-coating layer was used to promote the film buildup. This film assembling process, illustrated on Fig. 1b, was performed by electrochemically generating Cu(I) ions, allowing the occurrence of a Cu(I)-catalyzed alkyne–azide click reaction (CuAAC) between the building blocks.[24–26] Such an "electro-click" reaction allows the construction of polymeric,[26] organic[27] and inorganic[28] films on electrodes, including with supramolecular interactions[29] and with pattern control.[30,31] In this context, the physicochemical properties of electro-clicked hybridosome coatings are advancing the field of electro-synthesized films a step further, by enabling performing molecular encapsulation and subsequent stimuli-responsive release.

2. Results and discussion

2.1 Proof of concept

Both Hybridosome® nanocapsules and electro-click chemistry are emergent concepts useful for providing functional yet versatile materials.[21,26] Hybridosomes are a new class of hybrid nanocapsules that combine the features of both inorganic nanoparticles and the polymer chains contained in their shells. Here hybridosomes based on maghemite IONPs and PAA–C≡CH have been used as clickable building blocks.[32] In our previous work, such hybridosomes inherited magnetic properties from their IONP components, facilitating their purification.[23] Electro-click chemistry is now a recognized method for achieving a spatially confined covalent reaction between both organic and inorganic functional building blocks, resulting in the formation of engineered interfaces.[28,33–36] The concept introduced here is based on the assembly of hybridosome nanocapsules into covalent coatings by using the electro-click approach, while preserving the remarkable features of the hybridosomes. A 6% alkyne functionalized polyacrylic acid (PAA–C≡CH) (synthesis and characterization of the functional polymers is described in Schemes S1, S2 and Fig. S2, ESI†) was used to decorate the hybridosomes with click-suitable moieties. The resulting nanocapsules were covalently coupled with azide homobifunctional PEG linkers (N_3-PEG-N_3) in the vicinity of a PEI–C≡CH pre-coated FTO electrode (Fig. 1b). The local catalysis of the alkyne–azide Huisgen cycloaddition reaction was made possible by locally generating Cu(I) ions from Cu(II) in solution, by using cyclic voltammetry (CV). This process resulted in the construction of films composed of hybridosome nanocapsules covalently reticulated with PEG linkers.

Scanning electronic microscopy (SEM) investigations of the resulting electrodes reveal the stacking of several nanocapsules, forming a film (Fig. 1c) whose thickness, measured by atomic force microscopy (AFM) in the dried state, exceeded 850 nm after 800 CV cycles (Fig. 1d). Such a thickness value corresponds approximately to the stacking of 10 layers of hybridosomes since the dried nanocapsules, as seen by AFM, are approximately 70 nm thick. To demonstrate that this film construction can be attributed to the occurrence of the alkyne-azide Huisgen

cycloaddition between the functional building blocks, control experiments were performed (Fig. S3, ESI†). When one component required for the click reaction was removed, *i.e.* either the copper ions, the N_3-PEG-N_3 linkers or the CV required to generate the Cu(I) catalyst, no film construction was observed. This implies that the coating growth originates from the covalent "click" reaction between the functional hybridosomes and N_3-PEG-N_3 linkers.[26] To further confirm this trend, Attenuated Total Reflectance Fourier-Transform InfraRed spectroscopy (ATR-FTIR) was performed on the film and compared with the spectrum of its organic components, *i.e.* the N_3-PEG-N_3 linkers, the PAA–C≡CH from the clickable hybridosomes and the PEI–C≡CH from the pre-coating layer. The spectrum of the electro-clicked hybridosome coatings exhibited typical absorption bands of all these components, confirming their inclusion in the film (Fig. S4, ESI†). Interestingly, the intense absorption peak of the azide groups, visible on the spectrum of N_3-PEG-N_3 at 2100 cm^{-1}, was absent from the spectrum of the film, in contrast to the absorption peaks of the ethylene oxide group of PEG at 1060 cm^{-1}, further confirming the occurrence of the click reaction.[25,37]

2.2 Hybridosome® films construction and growth mechanism

The growth mechanism of the IONP-based hybridosome films was investigated by SEM microscopy after 25, 100 and 800 CV cycles (Fig. 2). At each stage, a rough evaluation of the film surface coverage was performed by thresholding the micrographs. Several germination points emerged at the early growth stages, achieving a surface coverage of around 11%, as calculated from Fig. 2a. When the buildup was allowed to proceed further, the film growth achieved percolation, reaching a surface coverage of 75% after 100 CV cycles (calculated from Fig. 2b) and above 90% after 800 cycles (calculated from Fig. 2c). In addition to this topological evolution, the thickness of the film increased to 850 nm after 800 CV cycles (Fig. 2d, e and Fig. S5, ESI†). The roughness of the films was estimated by calculating the RMS from the AFM data of the film thickness on covered areas (Table S1, ESI†). High roughness values were obtained which seem to correlate with the use of bifunctional PEG linkers, as was observed in our previous study and by El Haitami *et al.*[27,38] When the hybridosomes were adsorbed on the PEI–C≡CH coated electrode (0 CV cycles), the surface topography exhibited nodes around 70 nm thick corresponding to the thickness previously measured by AFM for single dried hybridosomes (Fig. 2d, black line). Single hybridosomes seem thus able to adsorb on the PEI–C≡CH-coated electrode in the absence of the electro-click reaction without leading either to any significant surface coverage or to the stacking of several nanocapsules (Fig. S3c, ESI†). In contrast, when the electro-click construction was performed for 25 CV cycles, the emergence of 200–300 nm thick structures was observed, suggesting that stacks of three to

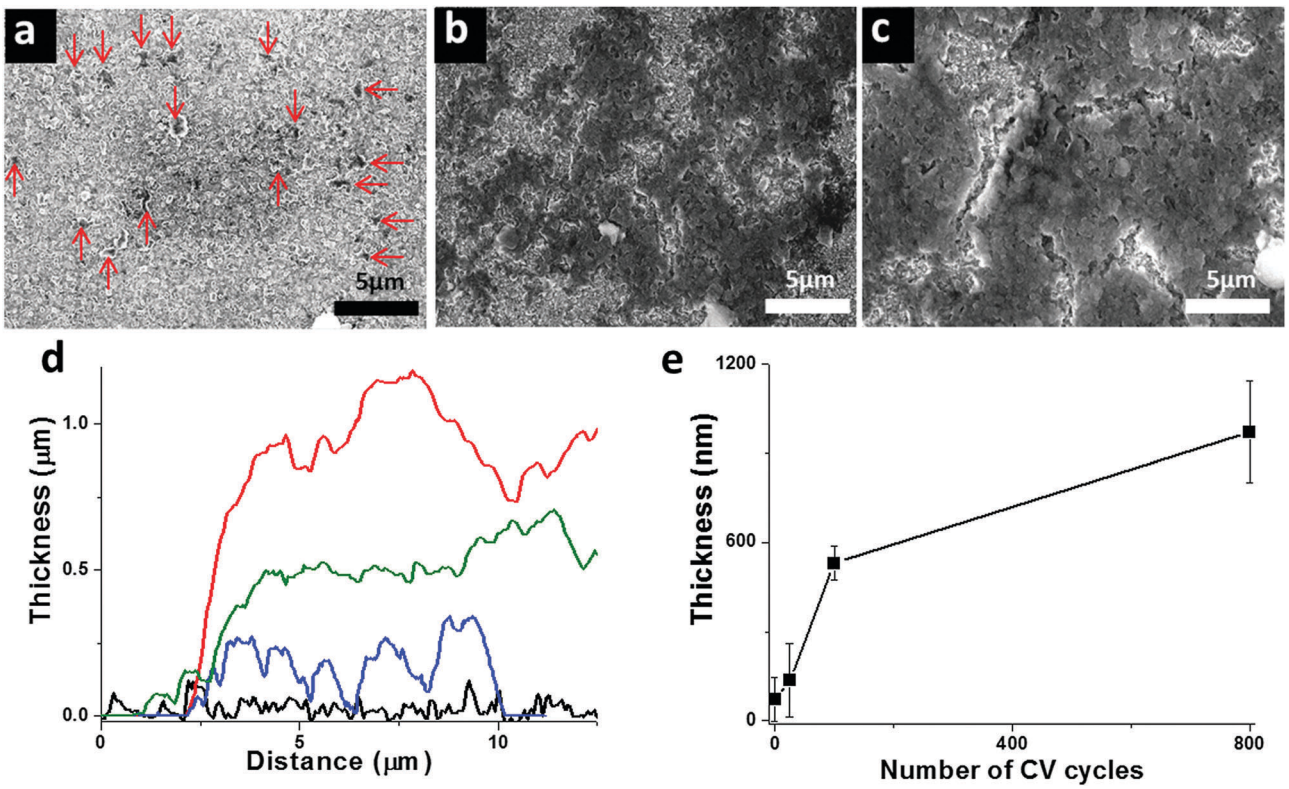

Fig. 2 Germination and growth of covalently reticulated Hybridosome® films. SEM micrographs of hybridosome films on FTO after 25 (a), 100 (b) and 800 (c) CV cycles (−0.2 V to 0.6 V *vs.* Ag/AgCl, 50 mV s^{-1}) in the presence of 4.5×10^9 hybridosomes per mL, 0.1 mg mL^{-1} N_3-PEG-N_3 and 0.6 mM $CuSO_4$ at pH 3.5. (d) Cross-sectional profiles of hybridosome films, measured by AFM in the dry state and contact mode, after 0 (black line), 25 (blue line), 100 (green line) and 800 (red line) CV cycles. (e) Evolution of the thickness of the corresponding films in the dry state.

four layers of hybridosomes had already formed (Fig. 2d, blue line). After a larger number of electro-click CV cycles, both the surface coverage and the thickness of the coating increased, reaching respectively 90% and 850 nm after 800 CV cycles in the dried state (Fig. 2d, green and red lines). At the same time, the intensity of the oxidation peak of copper on the electro-click voltammogram decreased with the number of cycles, indicating the insulating nature of the film, as expected for a polymer/maghemite composite film (Fig. S5, ESI†). These results are in accordance with previous studies where the electro-click construction relied exclusively on polymers. This confirms that the range of building blocks that can be used for assembling electro-clicked films can be extended to hybridosomes, leading to both the germination and growth of films based on multiple layers of covalently reticulated nanocapsules with both a tunable surface coverage and thickness.

2.3 Preservation of Hybridosome® properties in the film

Hybridosomes are promising building blocks for designing materials due to their chemical versatility,[32] their hybrid polymer/NP composition and their hollow structure. Preserving these features when the hybridosomes are integrated in electro-clicked coatings is thus desirable. The stability of the nanocapsules against the electrochemical conditions used for assembling the films was investigated by applying a CV to an IONP-based hybridosomes dispersion. The absence of any faradic current measured in the (−0.2 V to 0.6 V) CV window indicated the electrochemical stability of the hybridosomes (Fig. S7a, ESI†). The structural stability of these building blocks was investigated by measuring the size-distribution of the nanocapsules by SEM and scanning transmission electronic microscopy (STEM), both before and after their incorporation into the films (Fig. S7b, ESI†). The size distribution of the hybridosomes did not significantly change after their incorporation in the electro-clicked coatings with the average diameter increasing from 114 nm (+/−22 nm) to 122 nm (+/−21 nm). The hybridosome building blocks thus exhibit good structural tolerance to the electro-click synthesis conditions, leading to hybrid films with a hollow nanostructure. The chemical composition of the IONP-based hybridosome films was determined by using Energy Dispersive X-ray (EDX) spectroscopy (Fig. S8, ESI†). The detection of oxygen, carbon, nitrogen and iron indicate the presence of the polymeric (PAA–C≡CH, PEI–C≡CH, N_3-PEG-N_3) and inorganic (IONPs) components in the film. The hybrid nature of the electro-clicked hybridosomes films was thus confirmed. Since the hybridosomes can be synthesized by using a large range of NPs,[21] the transferability of this chemical versatility to the electro-clicked films was investigated. The possibility of assembling nanocapsule films based on a different choice of NPs would indeed open perspectives in several fields of applications including catalysis,[40–42] energy storage,[10,43] optoelectronics,[44] sensing[45] and controlled release[21,39] For example, another type of hybridosome has been synthesized by using CdSe@ZnS QD, IONPs and PAA–C≡CH as building blocks. The resulting hybridosomes exhibit the same morphology as nanocapsules entirely composed of IONPs. However, as expected, their EDX analysis indicates the presence of Zn, Se, Cd and S elements contained in the QDs (Fig. 3a). When such hybridosomes were used as building-blocks in the electro-click process, the coatings obtained presented similar morphological properties as films assembled from IONP-based hybridosomes (Fig. 3b). Chemical analysis of these films, by using EDX, revealed the presence of Fe, O, Zn, Se, S confirming the inclusion of both IONPs and CdSe@ZnS QDs in the coating. These results demonstrated how the films can inherit the chemical versatility of the hybridosomes and their nanostructural features.

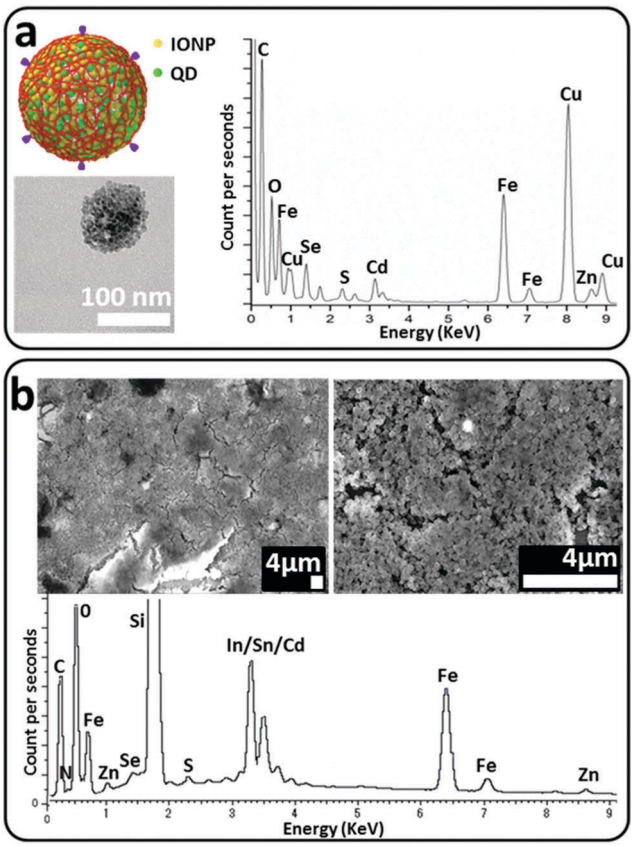

Fig. 3 Chemical composition of films based on QD-containing Hybridosomes®. (a) Schematic depiction, TEM micrograph and corresponding EDX analysis of hybridosome nanocapsules composed of CdSe@ZnS quantum dots (green), IONPs (yellow) and PAA–C≡CH (red). (b) SEM micrographs and EDX analysis of the corresponding films obtained after 800 CV cycles (−0.2 V to 0.6 V *vs.* Ag/AgCl, 50 mV s^{-1}) in the presence of 4.5×10^9 hybridosomes per mL, 0.1 mg mL^{-1} N_3-PEG-N_3 and 0.6 mM $CuSO_4$ at pH 3.5.

2.4 Encapsulation abilities of Hybridosomes®

The preservation of the hybridosome nanostructure in the interior of electro-clicked films suggests applications in several fields including the encapsulation and release of hydrophobic compounds.[21] As a proof of concept, a fluorescent bodipy probe was encapsulated into the hybridosomes during their synthesis. The UV-visible absorbance spectrum of the resulting bodipy-loaded hybridosome dispersion was compared with the spectrum of both bodipy and empty hybridosome dispersions in water (Fig. S9a, ESI†). Both bodipy-containing samples exhibited a similar UV-vis absorption spectrum marked by the emergence of two prominent absorbance bands localized at 502 nm and 532 nm.

These peaks were absent from the spectrum of empty hybridosome dispersions, suggesting that the encapsulation process was successful and did not significantly modify the chemical properties of the probe. The fluorescence properties of bodipy-loaded hybridosome dispersions were compared with the spectra of bodipy in a good solvent (tetrahydrofuran, THF) and in water where bodipy is poorly soluble (Fig. S9b, ESI†). A single fluorescence peak localized at 540 nm was observed for the well-dissolved bodipy in THF. In contrast, the spectrum of bodipy in water was marked by the emergence of 2 broad emission peaks at 560 nm and 625 nm, indicating the formation of *J*-aggregates.[46] Interestingly the spectrum of bodipy-loaded hybridosome dispersions exhibited a main peak around 540 nm and a shoulder around 565 nm, demonstrating that the encapsulation process largely inhibits the aggregation of bodipy (Fig. S9b, ESI†). The loading efficiency of bodipy in hybridosomes was estimated at *ca.* 73% from absorbance measurements at 540 nm (Fig. S10, ESI†). From this measurement, we calculate roughly that the stoichiometry is of 3 encapsulated bodipy molecules for 1 Fe atom. Importantly, when bodipy-loaded hybridosomes underwent further washings, the supernatant was completely clear of bodipy, indicating that the encapsulated dye does not leak spontaneously.

2.5 Features of bodipy-encapsulated Hybridosome® films

Using bodipy-loaded hybridosomes instead of "empty" nanocapsules for assembling the films did not change the morphology of the obtained coatings (Fig. 4a). To probe further the integrity of the hybridosomes integrated in electro-clicked films, the spectral features of bodipy-loaded hybridosome coatings were investigated in the dry state and compared with bodipy and bodipy-loaded nanocapsules drop-casted on FTO (Fig. 4b and c). On the one hand, the UV-vis absorbance spectra of all films exhibited similar characteristics with two prominent peaks at 502 nm and 532 nm, confirming the inclusion of bodipy in the films. Probe aggregation during drying was signalled by the appearance of a new absorption band at 680 nm (Fig. 4b). On the other hand, the fluorescence spectra of these films exhibited significant differences (Fig. 4c). The spectrum of the drop-casted bodipy films was comparable to the emission spectrum of bodipy in water, confirming that aggregation already was occurring in solution. However, bodipy-loaded hybridosomes films, either drop-casted or electro-clicked, exhibited a broad emission band around 565 nm, corresponding to the aggregate component already observed in the spectrum of bodipy-loaded hybridosome dispersions (Fig. 4c and Fig. S9b, ESI†). Free bodipy was thus absent from the hybridosome films, suggesting the absence of bodipy leaking from the nanocapsules during the electro-click process. These results confirm that the electro-click process with bodipy-loaded hybridosomes not only preserves the nanocapsule integrity but also its cargo content. The relationship between the composition of the building mixture and the resulting electro-clicked films was investigated by mixing both empty (E) and bodipy-loaded (L) hybridosome batches at different ratios. When the L/E ratio increased from 0% (pure empty hybridosomes) to 10%, 50% and 90%, a fluorescence emission peak emerged and increased in intensity between 660 and 670 nm,

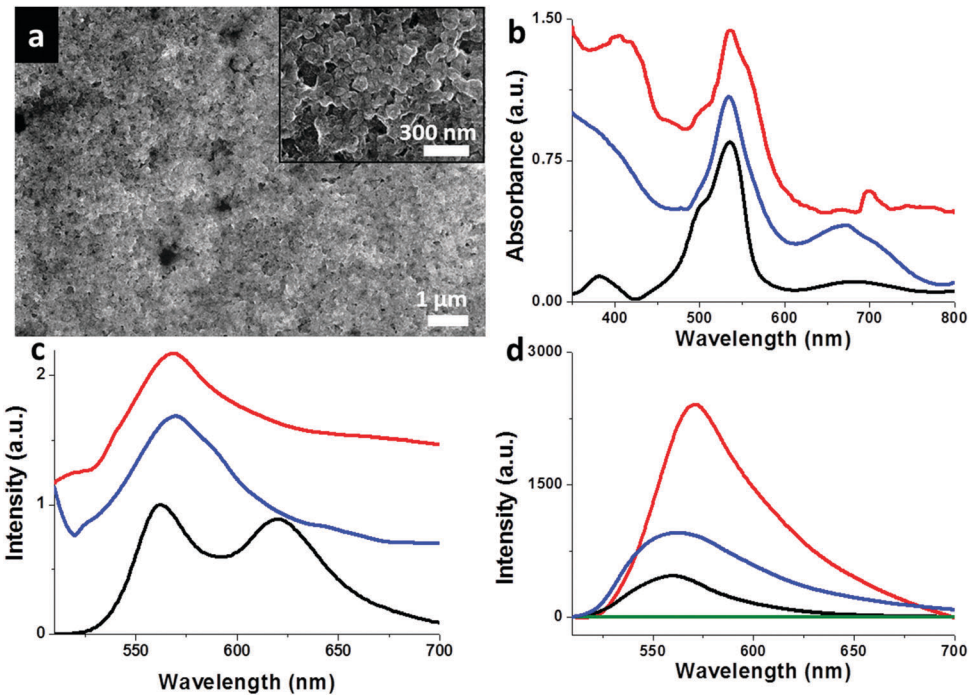

Fig. 4 Bodipy-encapsulated Hybridosome® films. (a) Typical SEM micrographs of bodipy-loaded hybridosome films after 800 CV cycles. (b) UV-visible absorbance spectra and (c) fluorescence spectra in the dry state (λ_{exc} at 480 nm) of bodipy (black line), drop-casted bodipy-loaded hybridosome (blue line) and an electro-clicked film based on bodipy-loaded hybridosomes (red line). (d) Fluorescence spectra in the dry state (λ_{exc} at 480 nm) of electro-clicked hybridosome films obtained from building mixtures containing 0% (green line), 10% (black line), 50% (blue line) and 90% (red line) bodipy-loaded hybridosomes.

demonstrating the presence of increasing quantities of bodipy in the films (Fig. 4d).

The area of the corresponding peaks increased accordingly, suggesting the absence of quenching when the L/E ratio was increased (Fig. S11, ESI†). The interaction of the fluorophore with itself seems thus to remain constant, supporting the hypothesis that the probe is encapsulated inside separated compartments within the film.[47] The simultaneous incorporation of several types of nanocapsules in the films, with a tunable ratio, seems thus possible. The hybridosome electro-clicked films constitute therefore a promising candidate for designing multiple-loaded coatings and multifunctional interfaces.

2.6 Stimulus-induced destabilization of Hybridosomes® films

The stability of the electro-clicked nanocapsules was probed by using pH drops as an external stimulus. The effect of decreasing the pH from pH 4 to pH 1 was first studied on hybridosome dispersions and resulted in a two-step destabilization. At pH 3, many nanocapsules were destabilized and were reorganized into larger structures up to several microns in size (Fig. S12, ESI†). pH 3 coincides with the full protonation point of the carboxylic groups of PAA chains, causing decreased polymer solubility in water, and reducing its ability to act as a colloidal stabilizer. This effect was recently reported as being responsible for the aggregation of PAA-coated silver and TiO_2 nanoparticles at acidic pH.[48,49] This destabilization of the hybridosome dispersions at pH 3 illustrates how these nanocapsules inherit the properties of their polymer component.[21] When the pH of hybridosome dispersions was decreased further to pH 1, the nanocapsules could no longer be observed and the morphology of the dispersed material dramatically changed (Fig. S12, ESI†). Although the IONPs composing the hybridosomes are thermodynamically unstable at both pH 1 and pH 3, their dissolution kinetic is faster at pH 1. This illustrates how the hybridosomes also inherit properties of their inorganic components.[50,51] The pH-sensitivity of the electro-clicked hybridosome films was also investigated at pH 3, 2.5 and 1, confirming the trend observed in dispersion (Fig. S13, ESI†). Interestingly, the coatings were destabilized after soaking for 15 min in a pH 2.5 solution instead of pH 3 for the nanocapsule dispersions. This suggests that the nanocapsules are better stabilized in the film environment. However, the aggregated hybridosomes were still clearly visible in the film at this pH value. In contrast, at pH 1, the morphology of the hybridosome films observed by SEM was marked by the absence of nanocapsules, in agreement with results obtained with the hybridosome dispersions.

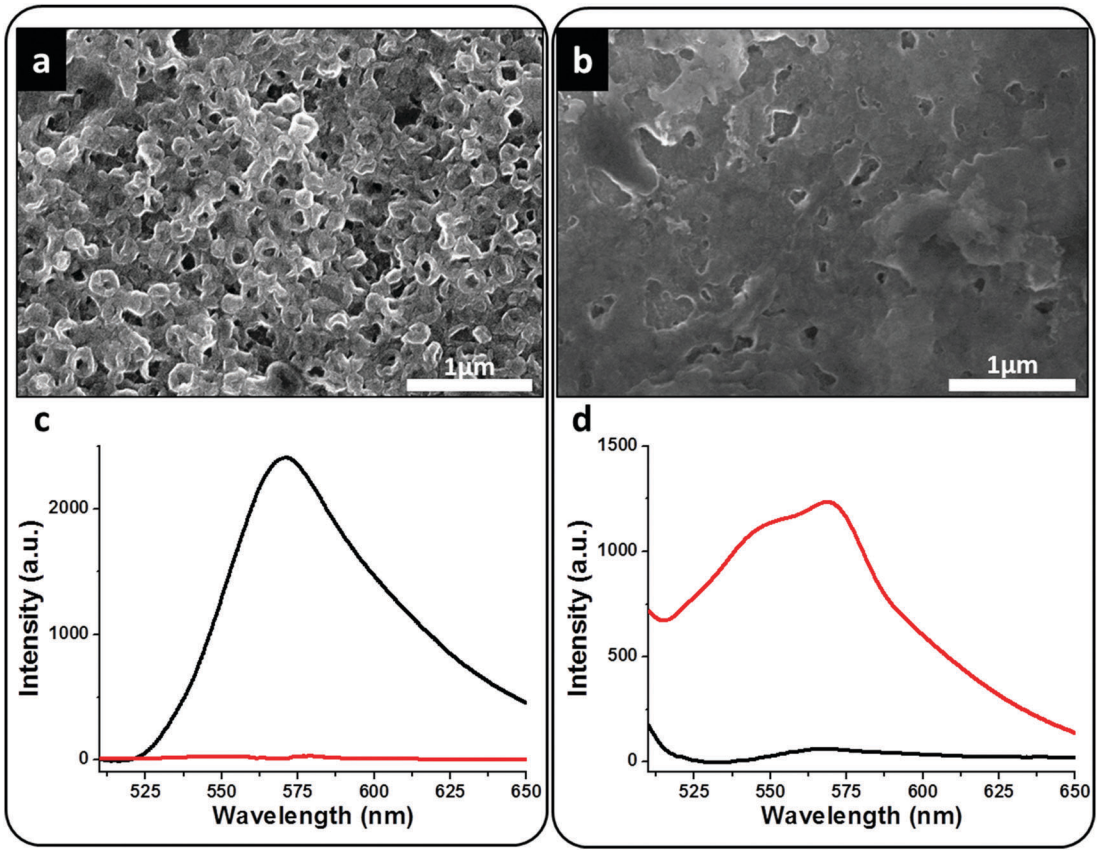

Fig. 5 Electro-triggered release abilities of electro-clicked Hybridosomes® films. SEM micrographs (a and b) and fluorescence spectra (λ_{exc} at 480 nm) in the dry state (c and d) of bodipy-loaded hybridosome films assembled on FTO (black line) and of the corresponding supernatant (red line) before (a and c) and after (b and d) application of +1 V potential (*vs.* Ag/AgCl) for 15 minutes in a 0.1 M NaCl solution.

2.7 Destabilization of bodipy-loaded Hybridosome® films

When bodipy-loaded nanocapsule films were brought into contact with a pH 1 HCl solution, the partial dissolution of the coating was also observed (Fig. S14a and b, ESI†). As a result, bodipy encapsulated in the film was released into the supernatant, which exhibited a fluorescence emission peak around 560 nm while the fluorescence of the film dramatically decreased (Fig. S14c and d, ESI†). By comparing the emission peak areas of the films before and after acidic treatment, the release rate of bodipy was estimated to exceed 95%. This result demonstrates the ability of the hybridosome films to encapsulate and release molecules upon a direct pH change of the environment. Since these films are electro-clicked on conducting substrates, the possibility of destabilizing the coating by an electrochemically-induced reduction of local pH was also investigated (Fig. 5). This approach, which consists of generating a proton gradient near the electrode by water electrolysis, has been reportedly used for the assembly and dissolution of the pH-sensitive polymer films.[52–54] Such a localized and easily controllable dissolution process is expected to trigger applications in the field of the localized release of medical drugs, for instance by using implantable microelectrodes.[55,56] A potential of +1 V (*vs.* Ag/AgCl, 0.1 M NaCl) was applied for 15 min to an electro-clicked hybridosome film constructed on FTO in order to generate a proton gradient at the electrode.[52] This treatment resulted in the destabilization of the coating as testified by the disappearance of the nanocapsules from the surface at a low SEM magnification (Fig. 5a and b). When higher magnifications were used, severely disorganized and fused hybridosomes were visible on SEM micrographs, leading to the loss of their nanostructure (Fig. S15, ESI†). This result was similar to the one obtained with hybridosomes dispersions at pH 3 and films soaked at pH 2.5 (Fig. S12 and S13, ESI†). Both the coated electrodes and their supernatant were studied by fluorescence spectroscopy (λ_{exc} at 480 nm) prior to and following the electrochemical stimulus. Before water electrolysis, no fluorescence was measured in the supernatant while the coated electrode exhibited an emission peak centered at 568 nm, indicating the presence of encapsulated bodipy (Fig. 5c, black line). After 15 min of water electrolysis, the fluorescence intensity of the electrode dramatically decreased while the supernatant exhibited two broad emission peaks centered at 550 and 570 nm indicating the release of aggregated bodipy in the aqueous supernatant (Fig. 5d). The release rate, estimated from the emission peak area of the film, exceeded 99%. These two methods for destabilizing electro-click hybridosome films suggest their application in the directed release of encapsulated molecules in response to either a global pH change or localized water electrolysis.

3. Conclusion

Nanocapsule films composed of hollow PAA/IONPs nanocapsules and PEG linkers were assembled on FTO electrodes by electro-click cross-linking of organic/inorganic Hybridosomes®. The growth of the film followed a germination/percolation mechanism, allowing tuning both the surface coverage (calculated from 520 μm^2 area micrographs) and the thickness of the films. After 800 CV cycles, a surface coverage exceeding 90% and a film thickness over 850 nm were achieved. This work clearly demonstrates that the mild physicochemical conditions required by the electro-click approach do not alter the chemical and structural properties of the hybridosome nanocapsules. Consequently, both the composition and the loading of the nanocapsules could be changed, demonstrating the versatility and encapsulation abilities of the hybridosome films. For example, a bodipy probe was successfully encapsulated in the hybridosomes and preserved upon the film construction. When a mixture of both bodipy-loaded and empty nanocapsules were used to assemble the film, the coating composition reflected the stoichiometry found in solution. The corresponding coatings could be destabilized by using either a pH or an electrochemical stimulus; releasing more than 95% of their fluorescent content within 15 min. By advancing the field of electro-synthesized films a step further toward the design of complex physicochemical interfaces, these results open perspectives for multifunctional coatings where a chemical versatility, a controllable stability and a hollow nanostructure are required.

4. Experimental

Materials

Copper sulfate pentahydrate ($CuSO_4 \times 5H_2O$, M = 249.7 g mol^{-1}, CAS 7758-99-8), branched polyethyleneimine (M = 25 kDa, CAS 9002-98-6), polyacrylic acid (M = 450 kDa, CAS 9003-01-4), amino-EG$_4$-alkyne (M = 231.3 g mol^{-1}, CAS 1013921-36-2), 10-undecynoic acid (M = 182.3 g mol^{-1}, CAS 2777-65-3), polyoxyethylene bis(azide) (M = 2050 g mol^{-1}, CAS 82055-94-5), benzotriazol-1-yloxy)tris(dimethylamino)phosphonium hexafluorophosphate (BOP, M = 442.28 g mol^{-1}, CAS 56602-33-6), *N*,*N*-diisopropylethylamine (DIEA, M = 129.24 g mol^{-1}, CAS 7087-68-5), *N*,*N*-dimethylformamide (DMF, M = 73.09 g mol^{-1}, CAS 68-12-2), and octadecylamine-coated CdSe@ZnS (product number 790 192) were purchased from Sigma-Aldrich and used as received. Tetrahydrofuran (THF, M = 72.10 g mol^{-1}, CAS 109-99-9) was purchased from VWR. Hydrochloric acid (HCl, M = 36.46 g mol^{-1}, CAS 7647-01-0), and sodium hydroxide (NaOH, M = 39.99 g mol^{-1}, CAS 122000-64-5) were purchased from Wako. 4,4-Difluoro-8-(4′-trimethylsilylethynylphenyl)-1,3,5,7-tetramethyl-2,6-diethyl-4-bora-3*a*,4*a*-diaza-*s*-indacene (bodipy, M = 476.2 g mol^{-1}) was kindly provided by O. Mongin (ISCR) and synthesized following a reported procedure.[57] FTO electrodes were purchased from ALS, Japan. All aqueous solutions were prepared with MilliQ water (18.2 MΩ cm^{-1}) purified using a Purelab Prima system.

Synthesis of functional polymers

The synthesis of PAA–C≡CH was adapted from our previous work and entails grafting amino-EG$_4$-alkyne on the polyacrylic acid backbone.[58] PAA (2 mmol) was dissolved in DMF (7 mL) with BOP (142 μmol) under stirring for 10 m. Amino-EG$_4$-alkyne

(108 μmol) was dissolved in DMF (5 mL) and DIEA (2 mmol) was added. After 90 minutes, the DMF was evaporated under reduced pressure. The residue was dissolved in milliQ water, and dialyzed (Spectra/Por, MWCO 12 kDa) against milliQ water for 48 h and recovered by evaporation under reduced pressure and freeze drying. The synthesis of PAA–C≡CH was performed by using an EDC/NHS approach. 10-Undecynoic acid (0.2 mmol) was dissolved in dichloromethane (7 mL) with 3-fold molar excess of (1-ethyl-3-(3-dimethylaminopropyl)carbodiimide hydrochloride and hydroxysuccinimide. After 10 minutes stirring, PEI (2 mmol) dissolved in dichloromethane (7 mL) was added and the reaction was allowed to proceed for 90 minutes. The dichloromethane was evaporated under reduced pressure. The residue was dissolved in milliQ water, dialyzed (Spectra/Por, MWCO 12 kDa) against milliQ water for 48 h and recovered by evaporation under reduced pressure and freeze drying. The functionalization degree of the obtained polymers was evaluated by using NMR spectroscopy (ESI†).

Preparation of iron oxide based Hybridosomes® and encapsulation step

The hybridosomes were elaborated as previously reported[21] by using PAA–C≡CH and the superparamagnetic iron oxide nanoparticles previously synthesized.[59] In a typical process, THF (100 μL) was added to a dispersion of iron oxide nanoparticles (m_{Fe} = 52.6 μg) followed by water (800 μL) then stirred. After 24 h, PAA–C≡CH (2.1 mM) was added to the mixture before solvent evaporation for 15 h at 40 °C. The resulting precipitate was magnetically attracted and dispersed in milliQ water (930 μL). The same procedure was used to synthesize mixed iron oxide (IONP)/quantum dot (QD) hybridosomes by initially mixing 50 μL (m_{Fe} = 26.3 μg) of the iron oxide (IONP) dispersion with 50 μL (m_{QD} = 25 μg) of the quantum dot (QD) dispersion in 100 μL of THF. The encapsulation of bodipy in hybridosomes was performed by adding 100 μL of a 1 mM bodipy in THF into 50 μL (m_{Fe} = 26.3 μg) of the initial iron oxide (IONP) suspension.

Film construction

ITO and FTO electrodes were cleaned by dipping in 0.1 M NaOH and 0.1 M HCl baths for 15 minutes followed by rinsing. A PEI–C≡CH pre-coating layer was deposited by dipping (10 mg mL^{-1}) for 15 minutes and subsequent rinsing. The film was constructed by applying a cyclic voltammetric current (−200 mV to +600 mV *vs.* Ag/AgCl at 50 mV s^{-1} under stirring) to the electrode in contact with a pH 3.5 solution containing typically 4.5 × 10 hybridosomes per mL, 0.6 mM $CuSO_4$ and 0.1 mg mL^{-1} N_3-PEG-N_3.

Film destabilization

Bodipy-loaded hybridosome films were first constructed by using 800 CV cycles. The resulting coated electrodes were either dipped in an HCl solution at the desired pH or subjected to a +1 V potential (*vs.* Ag/AgCl, in a 0.1 M NaCl buffer) for 15 minutes. The supernatant was analyzed directly after the process. The electrodes were rinsed with Milli-Q water and dried before analysis.

Cyclic voltammetry

A CHI model 613B potentiostat was used with a three-electrode apparatus based on an ITO and FTO coated quartz as the working electrode, a platinum wire as the counter electrode, and an RE1S Ag/AgCl-based reference electrode. The electrodes were purchased from ALS.

Fluorescence spectroscopy was performed using a JASCO FP8500 spectrofluorometer.

NMR analysis of the functionalized polymers PEI–C≡CH and PAA–C≡CH were performed in D_2O on a Bruker Avance III HD 500 MHz spectrometer fitted with a Dual $^1H/^{13}C$ probehead.

Atomic force microscopy (AFM) was performed by using an AFM SPA400-SPI4000 (Seiko Instruments Inc., Chiba, Japan) in contact mode and in the dried state with silicon nitride cantilevers, spring constant of 0.08 N m^{-1} (model SN-AF01S-NTK-W10200326 from Seiko Instruments). Height images were scanned at a fixed scan rate of 1 Hz. The thickness of the PEM films was measured by imaging the coatings after scratching. When possible, the AFM scanning direction was perpendicular to the scratch. Data evaluation was performed by using Gwyddion software. A plane-fit treatment was applied to the scratched area of each image, and its minimum height was set to z = 0.

Scanning electron microscopy (SEM), scanning transmission electron microscopy (STEM) and energy-dispersive X-ray spectroscopy (EDX) were performed using a Hitachi S-4800 at accelerating voltages of 30 kV. The samples were observed directly after 15 min drying under vacuum. The calculation of the hybridosome size distribution analysis and film surface coverage was performed from SEM and STEM data by using the ImageJ software.

Transmission electron microscopy (TEM), energy-dispersive X-ray spectroscopy (EDS) and tomography were performed using a JEM-2100 (JEOL) transmission electron microscope (accelerating voltage 200 kV) equipped with a CCD camera.

UV-visible spectroscopy was performed using a Shimadzu (Japan) UV visible NIR spectrophotometer (model UV-3600).

Attenuated total reflection infrared spectroscopy (ATR-FTIR) on the hybridosomes films and functionalized polymers was performed by using a Thermo Scientific Nicolet 4700 apparatus (USA).

Nanoparticle tracker analysis (NTA) tracks individual trajectories, allowing the calculation of the diffusion coefficient and thus of the hydrodynamic diameter of each particle. NTA was carried out with a Nanosight LM10 device system equipped with a 40 mW laser working at λ = 638 nm. Video sequences were recorded *via* a CCD camera operating at 30 frames per second and evaluated *via* the NANOSIGHT NTA 2.0 Analytical Software Suite. The hybridosome suspensions at [Fe] ∼ 50 μg mL^{-1} are washed two times after magnetic separation and diluted 100 times before NTA analysis.

Conflicts of interest

There are no conflicts to declare.

Acknowledgements

This work was supported by the JSPS KAKENHI Grant Number JP16H06518 (Coordination Asymmetry) and CREST, JST. F. S. warmly thanks the Embassy of France at Tokyo and MAEDI for travel and financial support and University Bretagne Loire and the Brittany region for the daily allowance financial support. G. R. thanks Dr Loic Jierry for fruitful discussions. The authors wish to acknowledge financial support of the Centre National de la Recherche Scientifique (CNRS, France) and of the Ministère de l'enseignement Supérieur la Recherche et de l'Innovation (France).

References

1 G. Decher, *Science*, 1997, **277**, 1232–1237.
2 C. D. Bain and G. M. Whitesides, *Science*, 1988, **240**, 62–63.
3 I. Rubinstein, S. Steinberg, Y. Tor, A. Shanzer and J. Sagiv, *Nature*, 1988, **332**, 426–429.
4 C. Li, H. Bai and G. Shi, *Chem. Soc. Rev.*, 2009, **38**, 2397–2409.
5 S. E. Fosdick, K. N. Knust, K. Scida and R. M. Crooks, *Angew. Chem., Int. Ed.*, 2013, **52**, 10438–10456.
6 G. Rydzek, T. G. Terentyeva, A. Pakdel, D. Golberg, J. P. Hill and K. Ariga, *ACS Nano*, 2014, **8**, 5240–5248.
7 C. Maerten, L. Jierry, P. Schaaf and F. Boulmedais, *ACS Appl. Mater. Interfaces*, 2017, **9**, 28117–28138.
8 G. Rydzek, Q. Ji, M. Li, P. Schaaf, J. P. Hill, F. Boulmedais and K. Ariga, *Nano Today*, 2015, **10**, 138–167.
9 N. Vogel, M. Retsch, C.-A. Fustin, A. del Campo and U. Jonas, *Chem. Rev.*, 2015, **115**, 6265–6311.
10 Y. Yue and H. Liang, *J. Power Sources*, 2015, **284**, 435–445.
11 K.-I. Min, G. Yun, Y. Jang, K.-R. Kim, Y. H. Ko, H.-S. Jang, Y.-S. Lee, K. Kim and D.-P. Kim, *Angew. Chem., Int. Ed.*, 2016, **55**, 6925–6928.
12 Y. Liu, B. Liu and Z. Nie, *Nano Today*, 2015, **10**, 278–300.
13 B. M. Teo, L. Hosta-Rigau, M. E. Lynge and B. Städler, *Nanoscale*, 2014, **6**, 6426–6433.
14 T.-L. Ha, J. Shin, C. W. Lim and I. S. Lee, *Chem. – Asian J.*, 2012, **7**, 36–39.
15 X. Lu, A. Xie, Y. Zhang, H. Zhong, X. Xu, H. Liu and Q. Xie, *Electrochim. Acta*, 2017, **249**, 79–88.
16 S. L. Hayward, D. M. Francis, M. J. Sis and S. Kidambi, *Sci. Rep.*, 2015, **5**, 14683.
17 N. Graf, E. Thomasson, A. Tanno, J. Voeroes and T. Zambelli, *J. Phys. Chem. B*, 2011, **115**, 12386–12391.
18 D. Volodkin, Y. Arntz, P. Schaaf, H. Moehwald, J.-C. Voegel and V. Ball, *Soft Matter*, 2008, **4**, 122–130.
19 K. Katagiri, R. Hamasaki, K. Ariga and J. Kikuchi, *J. Am. Chem. Soc.*, 2002, **124**, 7892–7893.
20 K. Katagiri, R. Hamasaki, K. Ariga and J. Kikuchi, *Langmuir*, 2002, **18**, 6709–6711.
21 F. Sciortino, G. Casterou, P.-A. Eliat, M.-B. Troadec, C. Gaillard, S. Chevance, M. L. Kahn and F. Gauffre, *ChemNanoMat*, 2016, **2**, 796–799.
22 F. Gauffre, F. Sciortino, G. Casterou, M. Kahn and S. Chevance, WO 2017103534 A2, 2017.
23 F. Sciortino, M. Thivolle, M. Kahn, C. Gaillard, S. Chevance and F. Gauffre, *Soft Matter*, 2017, **13**, 4393–4400.
24 N. K. Devaraj, P. H. Dinolfo, C. E. D. Chidsey and J. P. Collman, *J. Am. Chem. Soc.*, 2006, **128**, 1794–1795.
25 J. P. Collman, N. K. Devaraj, T. P. A. Eberspacher and C. E. D. Chidsey, *Langmuir*, 2006, **22**, 2457–2464.
26 G. Rydzek, L. Jierry, A. Parat, J.-S. Thomann, J.-C. Voegel, B. Senger, J. Hemmerlé, A. Ponche, B. Frisch, P. Schaaf and F. Boulmedais, *Angew. Chem., Int. Ed.*, 2011, **50**, 4374–4377.
27 G. Rydzek, P. Polavarapu, C. Rios, J.-N. Tisserant, J.-C. Voegel, B. Senger, P. Lavalle, B. Frisch, P. Schaaf, F. Boulmedais and L. Jierry, *Soft Matter*, 2012, **8**, 10336–10343.
28 G. Rydzek, D. Toulemon, A. Garofalo, C. Leuvrey, J.-F. Dayen, D. Felder-Flesch, P. Schaaf, L. Jierry, S. Begin-Colin, B. P. Pichon and F. Boulmedais, *Small*, 2015, **11**, 4638–4642.
29 G. Rydzek, T. Garnier, P. Schaaf, J.-C. Voegel, B. Senger, B. Frisch, Y. Haikel, C. Petit, G. Schlatter, L. Jierry and F. Boulmedais, *Langmuir*, 2013, **29**, 10776–10784.
30 W. F. Paxton, J. M. Spruell and J. F. Stoddart, *J. Am. Chem. Soc.*, 2009, **131**, 6692–6694.
31 C. Nicosia, S. O. Krabbenborg, P. Chen and J. Huskens, *J. Mater. Chem. B*, 2013, **1**, 5417–5428.
32 A. Glaria, M. L. Kahn, A. Falqui, P. Lecante, V. Collière, M. Respaud and B. Chaudret, *ChemPhysChem*, 2008, **9**, 2035–2041.
33 S. O. Krabbenborg, C. Nicosia, P. Chen and J. Huskens, *Nat. Commun.*, 2013, **4**, 1667.
34 N. Shida, Y. Ishiguro, M. Atobe, T. Fuchigami and S. Inagi, *ACS Macro Lett.*, 2012, **1**, 656–659.
35 G. De Leener, F. Evoung-Evoung, A. Lascaux, J. Mertens, A. G. Porras-Gutierrez, N. Le Poul, C. Lagrost, D. Over, Y. R. Leroux, F. Reniers, P. Hapiot, Y. Le Mest, I. Jabin and O. Reinaud, *J. Am. Chem. Soc.*, 2016, **138**, 12841–12853.
36 T. S. Hansen, J. U. Lind, A. E. Daugaard, S. Hvilsted, T. L. Andresen and N. B. Larsen, *Langmuir*, 2010, **26**, 16171–16177.
37 R. Kulbokaite, G. Ciuta, M. Netopilik and R. Makuska, *React. Funct. Polym.*, 2009, **10**, 771–778.
38 A. E. El Haitami, J.-S. Thomann, L. Jierry, A. Parat, J.-C. Voegel, P. Schaaf, B. Senger, F. Boulmedais and B. Frisch, *Langmuir*, 2010, **26**, 12351–12357.
39 Y. Chen, Q. Meng, M. Wu, S. Wang, P. Xu, H. Chen, Y. Li, L. Zhang, L. Wang and J. Shi, *J. Am. Chem. Soc.*, 2014, **136**, 16326–16334.
40 Z.-A. Qiao, P. Zhang, S.-H. Chai, M. Chi, G. M. Veith, N. C. Gallego, M. Kidder and S. Dai, *J. Am. Chem. Soc.*, 2014, **136**, 11260–11263.
41 J. Han, M. Wang, R. Chen, N. Han and R. Guo, *Chem. Commun.*, 2014, **50**, 8295–8298.
42 N. M. Sanchez-Ballester, G. Rydzek, A. Pakdel, A. Oruganti, K. Hasegawa, M. Mitome, D. Golberg, J. P. Hill, H. Abe and K. Ariga, *J. Mater. Chem. A*, 2016, **4**, 9850–9857.
43 X.-Y. Yu, L. Yu and X. W. D. Lou, *Adv. Energy Mater.*, 2016, **6**, 1501333.
44 G. Kang, J. Yoo, J. Ahn and K. Kim, *Nano Today*, 2015, **10**, 22–47.

45 L. Guo, J. A. Jackman, H.-H. Yang, P. Chen, N.-J. Cho and D.-H. Kim, *Nano Today*, 2015, **10**, 213–239.
46 S. Shimizu, A. Murayama, T. Haruyama, T. Iino, S. Mori, H. Furuta and N. Kobayashi, *Chem. – Eur. J.*, 2015, **21**, 12996–13003.
47 S. Acikgoz, G. Aktas, M. N. Inci, H. Altin and A. Sanyal, *J. Phys. Chem. B*, 2010, **114**, 10954–10960.
48 K. Kanehira, T. Banzai, C. Ogino, N. Shimizu, Y. Kubota and S. Sonezaki, *Colloids Surf., B*, 2008, **64**, 10–15.
49 Q. Huang, W. Shen, Q. Xu, R. Tan and W. Song, *Mater. Chem. Phys.*, 2014, **147**, 550–556.
50 J.-P. Jolivet, C. Chanéac and E. Tronc, *Chem. Commun.*, 2004, 481–487.
51 M. Baalousha, *Sci. Total Environ*, 2009, **407**, 2093–2101.
52 A. Dochter, T. Garnier, E. Pardieu, N. T. T. Chau, C. Maerten, B. Senger, P. Schaaf, L. Jierry and F. Boulmedais, *Langmuir*, 2015, **31**, 10208–10214.
53 K. Sadman, Q. Wang, S. H. Chen, D. E. Delgado and K. R. Shull, *Langmuir*, 2017, **33**, 1834–1844.
54 F. Boulmedais, C. S. Tang, B. Keller and J. Vörös, *Adv. Funct. Mater.*, 2006, **16**, 63–70.
55 O. Guillaume-Gentil, N. Graf, F. Boulmedais, P. Schaaf, J. Vörös and T. Zambelli, *Soft Matter*, 2010, **6**, 4246–4254.
56 N. Graf, F. Albertini, T. Petit, E. Reimhult, J. Vörös and T. Zambelli, *Adv. Funct. Mater.*, 2011, **21**, 1666–1672.
57 G. Ulrich and R. Ziessel, *J. Org. Chem.*, 2004, **69**, 2070–2083.
58 G. Rydzek, J.-S. Thomann, N. Ben Ameur, L. Jierry, P. Mésini, A. Ponche, C. Contal, A. E. El Haitami, J.-C. Voegel, B. Senger, P. Schaaf, B. Frisch and F. Boulmedais, *Langmuir*, 2010, **26**, 2816–2824.
59 G. Casterou, V. Collière, P. Lecante, Y. Coppel, P.-A. Eliat, F. Gauffre and M. L. Kahn, *Chem. – Eur. J.*, 2015, **21**, 18855–18861.

